Available online at www.sciencedirect.com
ScienceDirect
Trans. Nonferrous Met. Soc. China 30(2020) 3404−3416
Transactions of Nonferrous Metals Society of China
www.tnmsc.cn

# Numerical simulation and experimental verification of axial-directional crystallization purification process for high-purity gallium

You-dong DING[1,2], Lan JIANG[1,2], Zi-shen LI[1,2], Gao-feng FU[1,2], Liang YU[3]

1. Key Laboratory for Ecological Metallurgy of Multimetallic Mineral of Ministry of Education, Northeastern University, Shenyang 110819, China;
2. School of Metallurgy, Northeastern University, Shenyang 110819, China;
3. Key Laboratory of New Processing Technology for Nonferrous Metals & Materials of Ministry of Education, Guilin University of Technology, Guilin 541004, China

Received 8 July 2020; accepted 30 November 2020

**Abstract:** A transient numerical model was applied to simulating the axial-directional crystallization purification (ADCP) process of gallium (Ga) raw material at different coolant temperatures ($T_c$), and the evolutions of melt/crystal (m/c) interface shape, temperature distribution and thermal stresses were simulated and analyzed. The results showed that the m/c interface shape, temperature distribution, and thermal stress in the Ga material were determined by the $T_c$ in the crystallizer during the ADCP process. The temperature gradient and thermal stress in the grown Ga crystal increased with decreasing $T_c$. At $T_c$=15 °C, the m/c interface shape was flat, and the temperature gradient was ideal. Therefore, the Ga materials with lower thermal stresses and suitable m/c interface shape, and an ideal efficiency of impurity removal were obtained. The purity of Ga reached 6N standard by using ADCP process repeated 6 times at $T_c$ of 15 °C. The results of the simulation showed good agreement with the experimental results.

**Key words:** high purity Ga; axial-directional crystallization purification; finite element method

## 1 Introduction

Gallium (Ga) is an important semi-conductive material, being widely used in advanced semiconductor and photovoltaic devices [1]. The demands of high-purity (>99.9999%, 6N) Ga are increasing rapidly with the development of micro-electronics and optical component industry [2]. However, even very small amounts of impurities such as Cu, Pb, Fe, Mg, Zn and Cr in the 6N Ga can degrade or limit the electrical properties of the semiconductor devices [3].

Conventional refining methods such as electrolytic refining [4], zone refining [5], vacuum distillation [6], crystallization purification [7], and drawn single crystal have been applied for the preparation of 6N Ga [8]. The crystallization purification method has the advantages of low energy consumption, simple equipment, convenient operation, and short production cycle [9−11].

Based on the crystallization purification method, an axial-directional crystallization purification (ADCP) process is applied to prepare 6N Ga [12]. ADCP process is primarily characterized by its lower production cost and easier operation. The ADCP principle is based on the different solubilities of an impurity in the molten phase and solid phase of a base metal. This relation is called distribution coefficient ($k$) [13],

**Foundation item:** Project (51465014) supported by the National Natural Science Foundation of China; Project (Guike AA17204021-7) supported by the Innovation Driven Development Special Foundation of Guangxi, China
**Corresponding author:** Gao-feng FU, Tel: +86-13709818500, E-mail: fugf@smm.neu.edu.cn;
Liang YU, Tel: +86-13591633992, E-mail: 2010054@glut.edu.cn
DOI: 10.1016/S1003-6326(20)65471-1

which defines the purification degree that can be theoretically achieved in a system at equilibrium. This distribution coefficient can be taken from the binary phase diagram at a constant temperature, calculated as the relationship of the concentration of the impurity element in the solid phase ($C_S$) to its concentration on the molten phase ($C_L$) of the base metal [14]:

$$k=C_S/C_L \quad (1)$$

The lower the $k$ coefficient is than one, the larger the removal efficiency is via ADCP process. On the other hand, impurities with $k$ higher than one will tend to remain in the solid phase and be partially incorporated in the crystallized material. If an impurity has a $k$ coefficient close to one, it is not possible to be effectively removed via ADCP process.

Table 1 gives the theoretical $k$ values of impurities present in Ga. It can be seen from Table 1 that some impurities present in Ga have their $k$ values much lower than one, facilitating their removal by ADCP process. However, the impurities of Zn and Co have their distribution coefficient around 0.1, which can lead to a slow removal rate. It is known that the control of the temperature gradients in the crystal and the shape of crystallization front are important for purity and residual stresses in the crystal during ADCP process [15]. So, the heat transfer characteristics in Ga material during ADCP process are worthy of in-depth study [16]. However, it is difficult to measure and observe directly some important data, such as the temperature distribution, the shape and transformation of metal/crystal (m/c) interface, and the thermal stresses within Ga ingot during the ADCP process.

**Table 1** Distribution coefficients of several impurities in Ga

| Cu | Hg | Zn | Co | Pb | Sn | Ag |
|---|---|---|---|---|---|---|
| 0.025 | 0.014 | 0.145 | 0.310 | 0.011 | 0.049 | 0.044 |

Recently, the finite element method (FEM) is adopted to solve thermal stresses and the shape and transformation of m/c interface of Si and other elements, and to optimize material preparation techniques. DANILO et al [17] reported the numerical and experimental investigation of germanium refining via fractional crystallization based innovative rotary cooling device. BELLMANN et al [18] reported the optimization of silicon crystallization in a Bridgman growth furnace by numerical modeling. LU [19] reported the boundary element analysis of the heat transfer in Bridgman growth process of semi-transparent crystals. However, there are few studies on the heat transfer characteristics in Ga material during ADCP process. In this work, a transient numerical model was applied to simulating the ADCP process of 6N Ga and the evolution of temperature distribution, thermal stresses and shape of m/c interface were simulated and analyzed. Simulation results are confirmed by synthesis experiments.

## 2 Experimental

The ADCP process experiments are shown in Fig. 1, which provided the online measurement of the horizontal and vertical temperature gradient across the crystallizers. For the determination of the horizontal temperature gradient, three sets of thermocouples were placed in crystallizers. Within each set, two thermocouples (H-T1, H-T3) were 20 mm apart, with the middle thermocouple (H-T2) placed in the axisymmetric center of the crystallizers in Fig. 1(a). For the determination of the vertical temperature gradient, four sets of thermocouples were placed in crystallizers. Within each set, three thermocouples (V-T1, V-T2, V-T3) were 20 mm apart, with the fourth thermocouple (V-T4) placed 20 mm from the bottom of the crystallizers in Fig. 1(a). The crystallizer had flat bottom. Geometrical dimensions of the crystallizers are shown in Fig. 1(b). The crystallizers were made of Teflon. The bottom of the crystallizer was sealed with a 0.1 mm-thick Teflon film. The height of the liquid Ga is 90 mm.

The raw material is shown in Fig. 2. According to the National Standard for Industrial 4N Niall (GB T1475—2005), the impurity elements in 4N Ga were analyzed by ICP-OES. The results are given in Table 2, indicating that the purity of Ga is about 99.99%. The main impurity elements are Cu, Zn, Pb, Si, Co, Mn, and Cr. The content of the other elements is below the detection limit of ICP-OES.

Figure 3(a) shows the process of the simulation and experiment of 6N Ga preparation, and Fig. 3(b) shows the schematic diagram of the theoretical crystallization process during ADCP

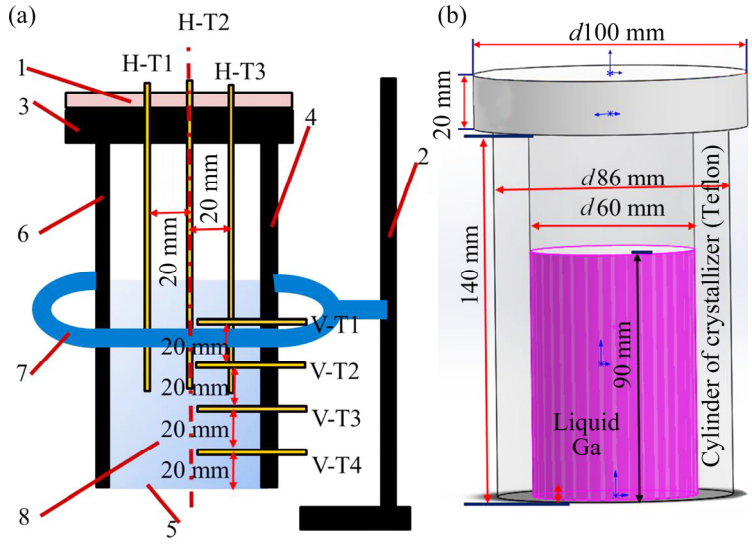


**Fig. 1** Schematic diagram (a) and dimensions (b) of crystallizers: 1−Thermometer support frame; 2−Crystallizer support; 3−Seal cover; 4−Scale; 5−0.1 mm-thick Teflon film bottom; 6−Cylinder insulation; 7−Support clamp; 8−Liquid Ga

**Fig. 2** Raw materials of 4N Ga used in experiment

**Table 2** Impurity element contents in 4N Ga raw material (mass fraction, $10^{-4}$)

| Cu | Zn | Pb | Si | Fe | Sn | Ni | Co | Mn | Mg | Cr |
|---|---|---|---|---|---|---|---|---|---|---|
| 4.0 | 0.6 | 2.3 | 0.6 | <0.5 | <0.5 | <0.5 | 0.7 | 0.6 | <0.5 | 0.7 |

process. According to the theoretical analysis of metal crystallization, the coolant temperature ($T_c$) must be kept in a certain range of low temperature for the liquid Ga, which can meet the supercooling of separation, purification, and keep the effective release of latent heat of crystallization [8]. A single stable longitudinal temperature gradient was established, the Ga solidified from bottom to top in the crystallizers, and the impurities in Ga segregated and enriched to the liquid Ga. The experiment steps are listed as follows [9].

(1) Crystallizers were washed with 3 mol/L HCl, deionized water (treated with ion exchange resin) and high-purity water (water resistivity is more than 18.25 MΩ·cm) for 3−5 times, and then the crystallizers were dried at 120 °C for 1 h.

(2) Raw materials of 4N Ga (1300−1500 g) was melted at 90 °C. The molten 4N Ga was transferred to a polytetrafluoroethylene beaker and mixed with 150 mL of 3 mol/L HCl at 60 °C for 1 h. The 4N Ga was washed with HCl, followed by washing with high purity water three times. The HCl was of high purity, and high purity water was used for preparation of HCl solution. After the molten 4N Ga was washed, it was transferred to the inner cavity of the crystallizers.

(3) The glycol water solution was used as coolant. The coolant was supplied using a constant low-temperature water tank with a built-in circulating water pump. The crystallizers were

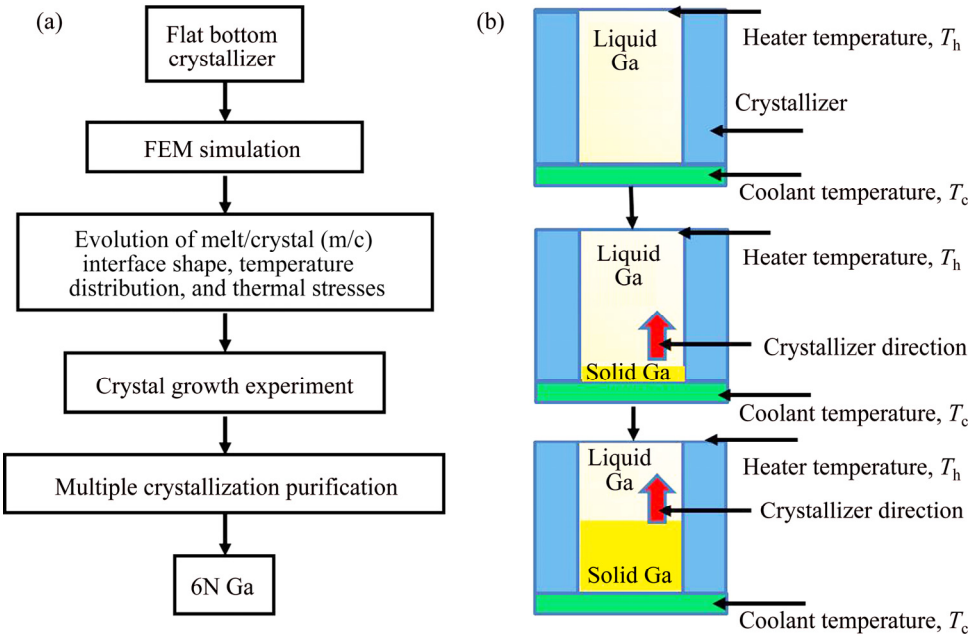


**Fig. 3** Schematic diagram of simulation and experiment of 6N Ga preparation: (a) Process flowchart; (b) Theoretical crystallization process during ADCP

clamped by support clamp, and the bottom of the crystallizer contacted the coolant. The $T_c$ was lower than the melting point of Ga (29.8 °C), which was 5, 7, 9, 11, 13 and 15 °C, respectively. The temperature control accuracy was ±1 °C. Thermocouples were used to monitor the coolant temperature.

(4) Thermocouples were installed in the crystallizer to monitor the temperature of liquid Ga and measure the horizontal and vertical temperature gradients of liquid Ga. Top surface temperature of liquid Ga was kept constant at 35 °C.

(5) The ADCP principle is based on the different solubilities of an impurity in the molten phase and solid phase of a base metal. When liquid 4N Ga was crystallized for a preset time, the impurities were concentrated in the remaining liquid Ga, while the amounts of impurities in solid gallium were reduced. The remaining liquid Ga was removed using a straw, and then hot (90 °C) water was introduced into the external cavity to remelt the solid Ga that had crystallized.

(6) The above crystallization process was repeated six times, and Ga with 6N purity was separated from impurities finally. Then, samples were collected and analyzed for their impurities.

The crystal growth rate measured in the experiment was the average crystal growth rate during the ADCP process of liquid Ga. When liquid Ga was crystallized for a preset time (0.5 or 1 h), the remaining liquid Ga was removed, and the calculation formula is as follows:

$$v=\frac{m_1-m_2}{t} \tag{2}$$

where $v$ is the average rate (kg/h); $m_1$ is the total mass of liquid Ga (kg); $m_2$ is the mass of remaining liquid Ga (kg); $t$ is the solidification time of liquid Ga (h); $(m_1-m_2)$ is the mass of solid Ga (kg).

In order to reduce the experimental error, each group of experiment was repeated three times, and the average value was taken.

## 3 Modeling

In order to study the effects of $T_c$ on the m/c interface shape, temperature distribution and thermal stress distribution, the 3D FEM transient heat transfer models of the crystallizers are established, as shown in Fig. 4.

The transient temperature and transient thermal stress distribution were calculated by FEM using the continuity equation, momentum equation, and energy equation. The equations which describe the heat and mass transfer phenomena during the crystallization process were expressed in the literatures [15−19]. The governing equations of the heat and mass transfer were solved with help of the

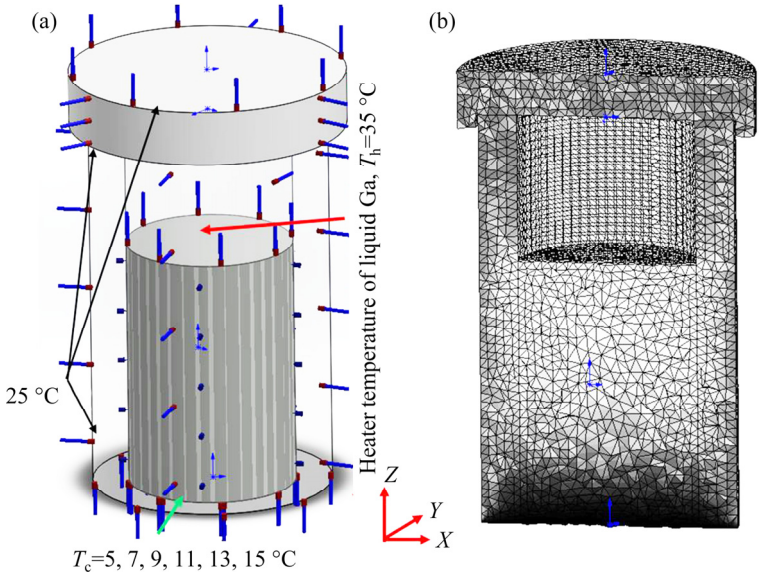


**Fig. 4** 3D FEM heat transfer model of crystallizer: (a) Boundary condition; (b) Cross-sectional view of mesh

SolidWorks2018 Simulation software [17,20].

To optimize computation and reduce computation time, the following assumptions were made:

(1) Ga melt flow was considered to be an incompressible axisymmetric Newtonian fluid.

(2) The surface of each component in the crystallizers was regarded as a diffuse gray reflective surface [15,18,19].

The transient thermal-mechanical coupling simulation was carried out, with the boundary conditions shown in Fig. 4(a), which included:

(1) The temperature of the outer crystallizer wall was 25 °C, and the crystallizer pressure was 0.1 MPa.

(2) $T_c$=5, 7, 9, 11, 13 and 15 °C, respectively.

(3) The heater temperature of the liquid Ga, $T_h$=35 °C.

(4) Total time of simulation, $t$=1 h, time step increment $\Delta t$=1 min; increment of minimal initial time, $\Delta t_{min}$=0.1 min.

The cross-sectional view of the mesh-generated model is shown in Fig. 4(b). The standard grid and Jacobi 4 point solid grid model were adopted. To ensure the calculating efficiency and precision, a mesh automatic transition method was adopted. The element size was 3 mm, the tolerance was 0.15 mm and the maximum height to width ratio was 4.24. The model was meshed into 187354 elements and 266560 nodes for crystallizer, respectively. The material physical properties of the crystallizer components are given in Table 3.

**Table 3** Typical physical properties of crystallizer components

| Material | Variable | Value |
|---|---|---|
| Liquid Ga | Density/(g·cm$^{-3}$) | 6.114 |
| | Thermal conductivity/(W·m$^{-1}$·°C$^{-1}$) | 38.3 |
| | Heat capacity/(J·g$^{-1}$·°C$^{-1}$) | 0.39 |
| Crystal Ga | Density/(kg·m$^{-3}$) | 5.907 |
| | Thermal conductivity/(W·m$^{-1}$·°C$^{-1}$) | 40.6 |
| | Heat capacity/(J·g$^{-1}$·°C$^{-1}$) | 0.37 |
| | Melting heat/(kJ·mol$^{-1}$) | 5.59 |
| Teflon (Cylinder of crystallizer) | Density/(g·cm$^{-3}$) | 2.20 |
| | Thermal conductivity/(W·m$^{-1}$·°C$^{-1}$) | 0.25 |
| | Surface tension/($10^{-3}$ N·m$^{-1}$) | 18 |
| | Tensile strength/MPa | 35 |
| | Elongation/% | 200 |
| | Tensile modulus/GPa | 400 |
| | Bending modulus/MPa | 420 |
| | Compression elastic modulus/GPa | 500 |
| | Linear expansion coefficient/($10^{-5}$ °C$^{-1}$) | 10 |

## 4 Results and discussion

### 4.1 Simulation results

Figure 5 shows the m/c interface shapes of isothermal 29.8 °C (melting point of Ga) and temperature distribution in crystallizer at different $T_c$ for crystallization time of 1 h during the ADCP process.

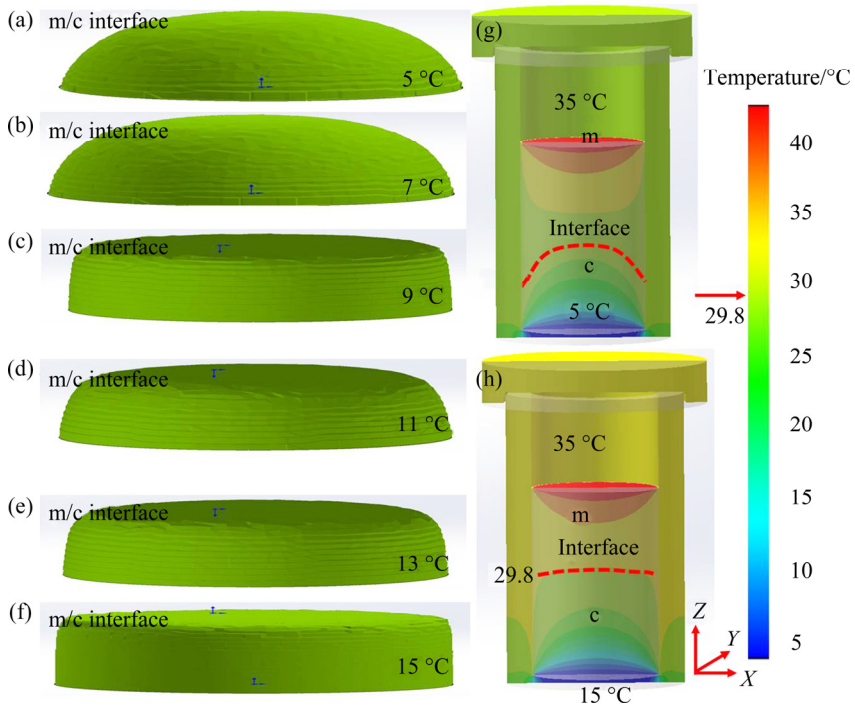


**Fig. 5** Calculated m/c interface shapes of isothermal 29.8 °C (a−f) and temperature distributions (g, h) in crystallizer at different $T_c$ for crystallization time of 1 h

Figures 5(a,b) show that the m/c interface shape was severely convex to the Ga melt at $T_c$ of 5 and 7 °C. Reducing the $T_c$ enhanced the heat dissipation capacity of the hot zone in the crystallizers. At lower $T_c$, the temperature gradient inside the liquid Ga was higher. The positive temperature gradient was formed at this time, and the temperature at the front of the m/c interface was higher in the radial direction of the crystallizer, hindering the release of latent heat of crystallization in this direction, and thus decreasing the crystal growth in this direction [21].

Figures 5(c−e) show that the m/c interface shape was convex to the Ga crystal at $T_c$ from 9 to 13 °C. The pyramid tip of Ga crystal became obvious, attributed to the fact that as the crystallization continued, impurity elements constantly accumulated in the Ga liquid, and the impurity content at the m/c interface increased, which enhanced the probability of impurity elements attaching to the growth tip of Ga crystal [22]. Owing to the difference in the atomic radius and electronegativity between Ga and impurity elements, the impurity atoms attached to the growth tip entered into the Ga lattice or lattice gap, causing the growth defect of Ga crystal. This indicated that the removal of impurity elements decreased with the progress of crystallization and was consistent with the literatures [23,24].

Figure 5(f) shows that m/c interface shape was flat at $T_c$ of 15 °C, indicating that the temperature gradient formed could release the latent heat of crystallization generated during the crystal growth to the front of the m/c interface, and transferred and released it outwardly along the direction of temperature gradient. The m/c flat or slightly convex interface shape was beneficial to the enrichment of impurity elements from the m/c interface to the liquid phase, thereby affording the Ga solid metal with higher purity [25].

Figures 5(g, h) show temperature distribution in crystallizer at different $T_c$ for crystallization time of 1 h during the ADCP process. As can be seen, the temperature field distribution was consistent. The red dotted line in Figs. 5(g, h) represents the m/c interface shapes of isothermal 29.8 °C (melting point of Ga).

Figure 6 shows the average temperature gradients within the Ga melt at different $T_c$ for crystallization time of 1 h during the ADCP process in crystallizer. The calculated average temperature gradient was from about 1.78 °C/mm in Fig. 6(a) to 1.04 °C/mm in Fig. 6(f) with $T_c$ from 5 to 15 °C. The heat flow was driven by the vertical

temperature gradient caused by the differences in thermal conductivities of Ga melt and crystal. This demonstrated that the configurations of the crystallizers increased the vertical heat diffusion, and the heat diffusion also increased from the Ga crystal domain to the flat bottom of the crystallizers.

Figure 7 shows the *Z*-axis temperature gradients within the Ga melt at different $T_c$ for crystallization time of 1 h during the ADCP process.

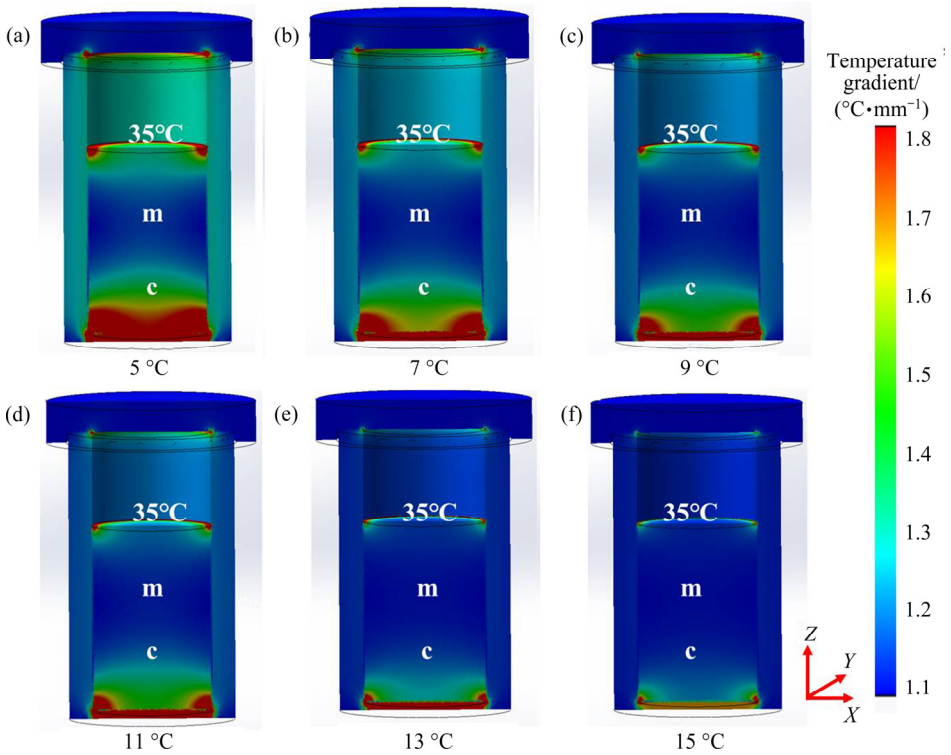


**Fig. 6** Calculated average temperature gradient distributions in crystallizer at different $T_c$ for 1 h crystallization: (a) 5 °C; (b) 7 °C; (c) 9 °C; (d) 11 °C; (e) 13 °C; (f) 15 °C

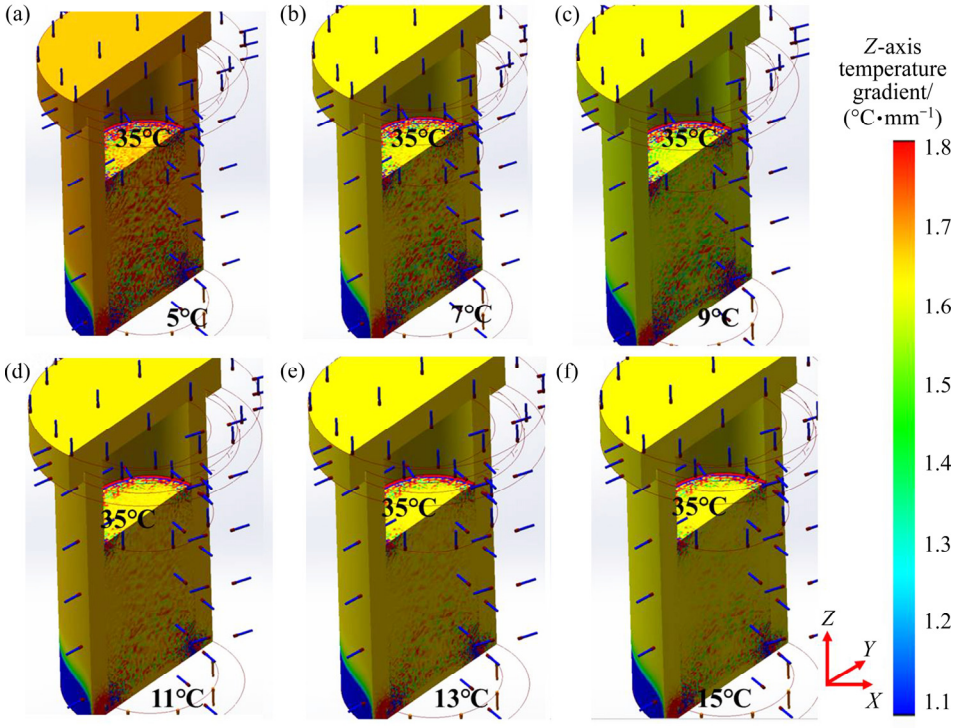


**Fig. 7** Calculated *Z*-axis temperature gradient distributions in crystallizer at $T_c$ for 1 h crystallization: (a) 5 °C; (b) 7 °C ; (c) 9 °C; (d) 11 °C; (e) 13 °C; (f) 15 °C

It should be noted that an increased *Z*-axis temperature gradient in the Ga melt could be achieved by reducing the $T_c$. The heat flow was driven by the vertical temperature gradient caused by the differences in thermal conductivities of Ga melt and Ga crystal. The calculated average temperature gradient was from about 1.86 °C/mm in Fig. 7(a) to 1.24 °C/mm in Fig. 7(f) with $T_c$ from 5 to 15 °C. Calculated results indicated that *Z*-axis temperature gradient was 1.24 °C/mm in Fig. 7(f) at $T_c$ of 15 °C, which might be beneficial to reducing the thermal stress.

Figures 8 shows the *X*-axis temperature gradients within the Ga melt at different $T_c$ for crystallization time of 1 h during the ADCP process. The calculated *X*-axis temperature gradient was from about 0.34 °C/mm in Fig. 8(a) to 0.018 °C/mm in Fig. 8(f) at $T_c$ from 5 to 15 °C. An increased horizontal temperature gradient in the Ga melt could be achieved by reducing the $T_c$. It should be noted that the temperature gradient in the vertical direction was obviously greater than that in the horizontal direction. It can be deduced that the Ga crystals were completely in the way of layer-by-layer promotion growth. The crystal growth process might be accompanied by very small amount of dendrite or peritectic formation, and the purification was improved in Ga solid at $T_c$ of 15 °C because it had the smallest horizontal temperature gradient.

The von Mises stress is one of main factors that affect the generation and multiplication of dislocation. Figure 9 shows the Von-Mises thermal stress distributions within the Ga melt at different $T_c$ for crystallization time of 1 h. From the simulation results, $T_c$ significantly affected the von Mises stress. The calculated highest thermal stress was from 0.95 MPa in Fig. 9(a) to 0.12 MPa in Fig. 9(f) with $T_c$ from 5 to 15 °C. The highest thermal stress was only 0.12 MPa at $T_c$ of 15 °C in Fig. 9(f), and might be beneficial to purity improvement of Ga crystal.

The maximum principal stress is also one of the factors that affect the generation and multiplication of dislocation in Ga ingot. Figure 10 shows the maximum principal stress distributions in Ga ingot. From the simulation results, it was concluded that $T_c$ significantly affected the principal

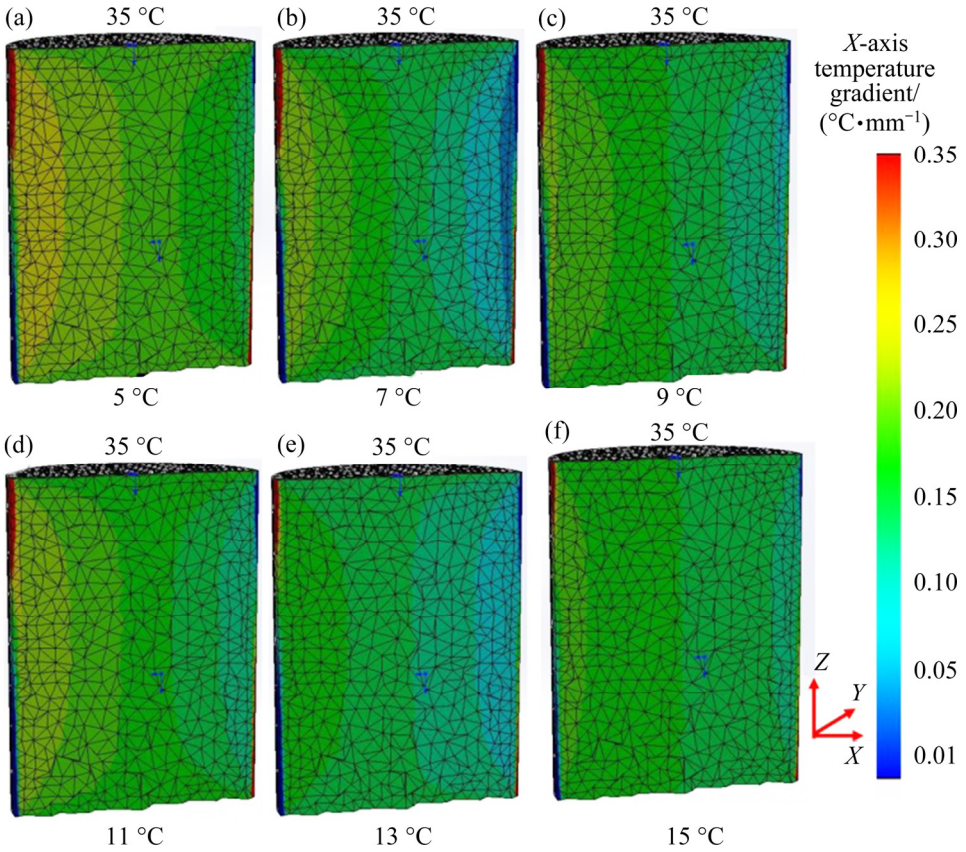


**Fig. 8** Calculated *X*-axis temperature gradient distributions in crystallizer at $T_c$ for 1 h crystallization: (a) 5 °C; (b) 7 °C ; (c) 9 °C; (d) 11 °C; (e) 13 °C; (f) 15 °C

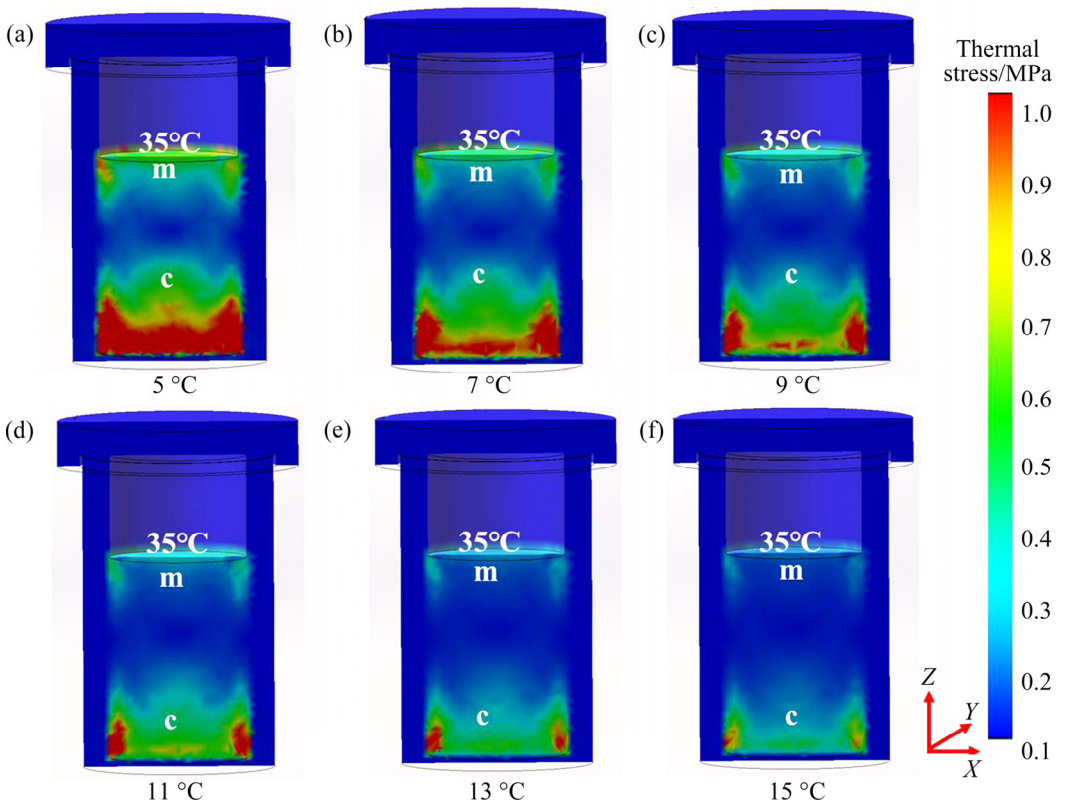


**Fig. 9** Calculated von Mises stress distributions in crystallizer at different $T_c$ for 1 h crystallization: (a) 5 °C; (b) 7 °C; (c) 9 °C; (d) 11 °C; (e) 13 °C; (f) 15 °C

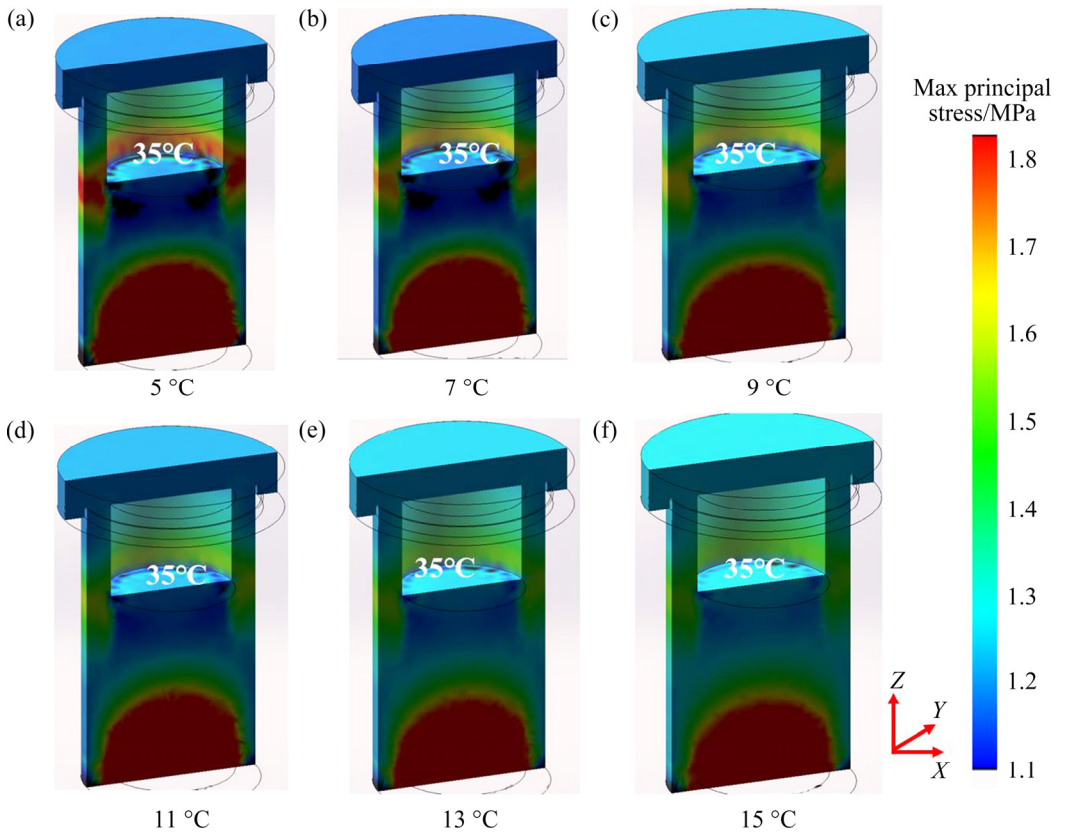


**Fig. 10** Calculated maximum principal stress distributions in crystallizer at different $T_c$ for 1 h crystallization: (a) 5 °C; (b) 7 °C; (c) 9 °C; (d) 11 °C; (e) 13 °C; (f) 15 °C

stress. The highest thermal stress calculated was from 1.75 MPa in Fig. 10(a) to 1.63 MPa in Fig. 10(f) with $T_c$ from 5 to 15 °C. The maximum principal stress in Ga ingot at $T_c$ of 15 °C was lower compared to that at $T_c$ from 5 to13 °C. The variation of the principal stress was found at the top of the Ga ingot. The principal stress was concentrated at the bottom of the crystallizer, which would promote nucleation and growth of Ga crystal. The lower value of the principal stress would reduce the generation of dislocations and defects, which might be beneficial to purity improvement of Ga crystal. So, the crystal quality was improved at $T_c$ of 15 °C.

WANG et al [26] reported that the shear stress causes the generation of dislocations and defects in grown silicon ingots. HOSHIKAWA et al [27] reported that the shear stress causes the generation of dislocations and defects in vertical Bridgman growth of sapphire-seed crystals. These studies show that shear stress would reduce the purification efficiency of crystals. Therefore, it is necessary to calculate the influence of $T_c$ on the shear stress in Ga ingot and select the suitable $T_c$ with the minimum shear stress. Figure 11 shows the calculated maximum shear stress distributions of Ga ingot. From the simulation results, it was concluded that $T_c$ significantly affected the shear stress. The highest thermal stress calculated was from 0.78 MPa in Fig. 11(a) to 0.69 MPa in Fig. 11(f) with $T_c$ from 5 to 15 °C. Shear stress was diffusely distributed in Ga ingot and would reduce generation of dislocations and defects, which was beneficial to purity improvement of Ga crystal. The maximum shear stress in Ga ingot at $T_c$ of 15 °C was lower than that at $T_c$ from 5 to13 °C. So, the Ga crystal quality was improved at $T_c$ of 15 °C.

The experimental data of temperature gradient in crystallizer are given in Table 4. The experimental $Z$-axis temperature gradient was from about 1.88 to 1.25 °C/mm with $T_c$ from 5 to 15 °C. The experimental $X$-axis temperature gradient was from about 0.36 to 0.02 °C/mm with $T_c$ from 5 to 15 °C. It is indicated that temperature gradient of $Z$-axis is greater than that of $X$-axis. The experimental results correlate well with the simulation results shown in Figs. 6−8.

### 4.2 Morphology of Ga crystal

Figure 12 shows that at different $T_c$, the morphology of Ga crystal exhibited a distinct “shell

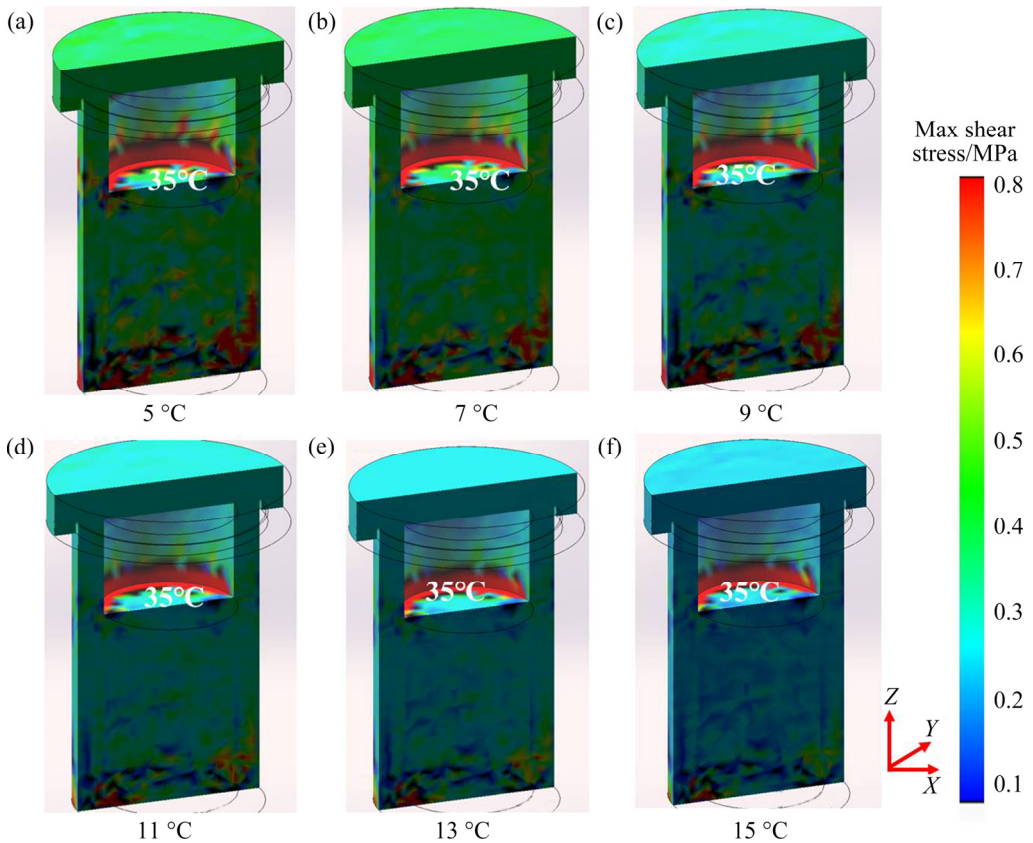


**Fig. 11** Calculated maximum shear stress distributions in crystallizer at different $T_c$ for 1 h crystallization: (a) 5 °C; (b) 7 °C; (c) 9 °C; (d) 11 °C; (e) 13 °C; (f) 15 °C

**Table 4** Experimental data of temperature gradient in crystallizer

| $T_c$/°C | $T_h$/°C | $Z$-axis temperature gradient/(°C·mm$^{-1}$) | $X$-axis temperature gradient/(°C·mm$^{-1}$) |
|---|---|---|---|
| 5 | 35 | 1.88 | 0.36 |
| 7 | 35 | 1.71 | 0.27 |
| 9 | 35 | 1.48 | 0.20 |
| 11 | 35 | 1.39 | 0.18 |
| 13 | 35 | 1.36 | 0.10 |
| 15 | 35 | 1.25 | 0.02 |

pattern" with uniform grain spacing. This indicates that the Ga crystal grew in the layer-by-layer manner, which was favorable for removing the impurity [14]. It is also found that the solidified structure exhibited the geometric polyhedron shape characteristics, indicating that its growth mode changed from dendrite growth to lamellar growth.

The higher heat transfer efficiency at the bottom of the crystallizer would lead to changes of the crystal morphology and presence of a large number of irregular growth steps at $T_c$ of 5 °C in Fig. 12(a) compared to those at $T_c$ of 7 °C in Fig. 12(b). It can be deduced that the crystals were not complete in the way of layer-by-layer growth, and the crystal growth process might be accompanied by dendrite or peritectic formation, which would envelope liquid phase, entrap impurities, and reduce purification effect in Ga solid at $T_c$ from 5 to 7 °C.

The crystal growth rate was slower at $T_c$ of 9 °C slightly than that at $T_c$ from 5 °C in Fig. 12(a) to 7 °C in Fig. 12(b), and the crystal morphology displays a distinct narrow "shell pattern". This suggested that at $T_c$ of 9 °C, the Ga crystals grew in the layer-by-layer manner, which was favorable for the removal of impurities.

The crystal growth rate was slower at $T_c$ from 11 °C in Fig. 12(e) to 15 °C in Fig. 12(f) than that at $T_c$ of 9 °C. The crystal morphologies also displayed distinct "shell pattern" [28]. However, it was found that "shell pattern" in Fig. 12(f) was smoother and more uniform than the others. It can be concluded that the Ga crystals grew in the layer-by-layer manner and the crystal morphology displayed a distinct narrow "shell pattern" at $T_c$ of 15 °C, which was favorable for the removal of impurity.

### 4.3 Purification of Ga crystal

The impurity contents in high-purity Ga prepared during the ADCP process were tested. The determination method followed high purity Gallium chemical analysis method (YS/T 474—2005) for the determination of trace elements by inductively coupled plasma mass spectrometry (ICP-MS). Based on the above studies, the optimum technological parameters during the ADCP process of 4N raw material Ga were determined at $T_c$ of 15 °C. It is known that the repeated ADCP process can improve the purity of Ga material. In order to

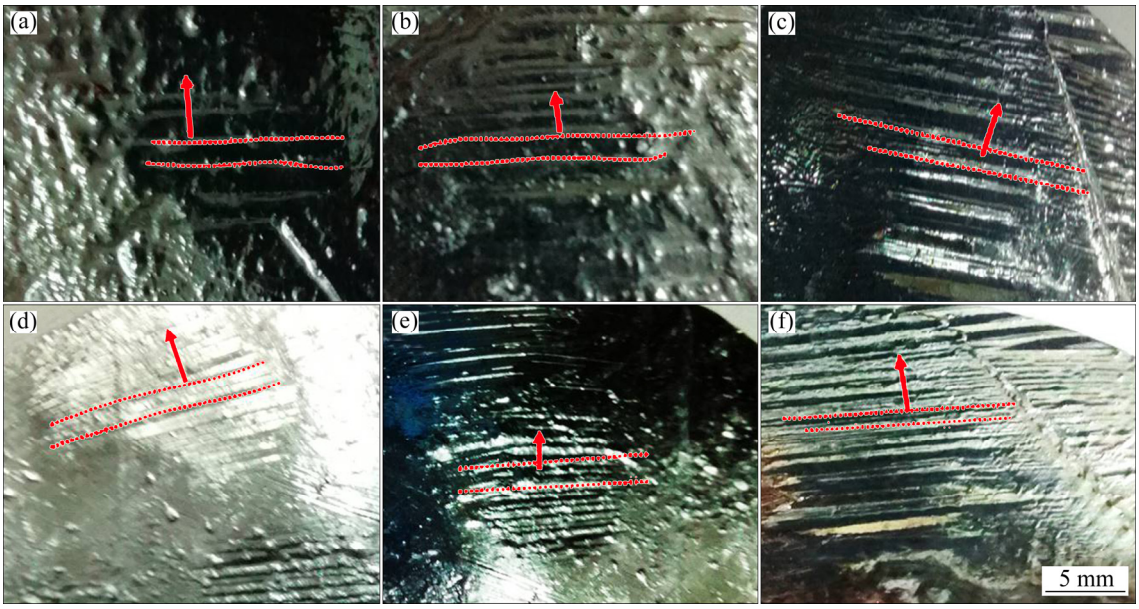


**Fig. 12** Morphologies of Ga crystals prepared in crystallizers crystallized at different $T_c$ for 1 h: (a) 5 °C; (b) 7 °C; (c) 9 °C; (d) 11 °C; (e) 13 °C; (f) 15 °C

compare the effects of different $T_c$ on the purification, the purity of Ga was tested at $T_c$ of 9 °C as well. The impurity contents in high-purity Ga prepared during the ADCP process repeated for 6 times were tested. The results are given in Table 5.

It can be seen from Table 5 that the contents of impurities in Ga dropped to a very low level during the ADCP process repeated for 6 times. The contents of impurities except Fe were lowered below the detection limit. The impurities, such as Cu, Pb and Sn, present in Ga had their distribution coefficient $k$ values much lower than 1, dropped to a very low level by ADCP process.

**Table 5** Impurity contents in Ga material tested by ICP-MS after ADCP process at $T_c$ of 9 and 15 °C repeated 6 times (mass fraction, $10^{-6}$)

| $T_c$ | Cu | Zn | Pb | Si | Fe | Sn |
|---|---|---|---|---|---|---|
| 9 | <0.2 | <1.0 | <0.3 | <0.5 | 0.8 | <0.5 |
| 15 | <0.2 | <1.0 | <0.3 | <0.5 | 0.6 | <0.5 |

| $T_c$ | Ni | Co | Mn | Mg | Cr |
|---|---|---|---|---|---|
| 9 | <0.8 | <1.0 | <0.2 | <0.5 | <0.5 |
| 15 | <0.8 | <1.0 | <0.2 | <0.5 | <0.5 |

The contents of impurities, such as Zn and Co, present in Ga have their $k$ values around 0.1, which can lead to a slower removal rate, however, the content of Zn and Co dropped to a very low level during the ADCP process repeated 6 times.

Therefore, it can be concluded $T_c$ of 15 °C is beneficial for purity improvement of crystal Ga.

The impurity content of Fe ($0.6\times10^{-6}$) is higher than that of other elements, which may be caused by the used appliances during the experiments. It has also been reported in other papers [28].

According to the National Standard for Industrial (GB T10118—2009), it has reached the high purity Ga-06 standard, which proving the effectiveness of the simulation results to obtain the best parameters for Ga crystallization.

## 5 Conclusions

(1) The m/c interface shape was severely convex to the Ga melt at $T_c$ of 5 and 7 °C, while it was convex to the Ga crystal at $T_c$ from 9 to 13 °C.

(2) The thermal conditions provided ideal temperature gradient in the Ga with lower thermal stresses, suitable flat m/c interface and an ideal efficiency of the impurity removal at $T_c$ of 15 °C.

(3) At $T_c$ of 15 °C, the Ga crystals grew in the layer-by-layer manner and the crystal morphology displayed a distinct narrow “shell pattern”, which was favorable for the removal of impurity.

(4) The purity of Ga reached 6N standard by using ADCP process repeated for 6 times at $T_c$ of 15 °C and the simulation results were confirmed by the experiments.

## References

[1] CHOU Wei-Lung, WANG Chih-Ta, YANG Kai-Chiang, HUANG Yen-Hsiang. Removal of gallium(III) ions from acidic aqueous solution by supercritical carbon dioxide extraction in the green separation process [J]. Journal of Hazardous Materials, 2008, 160: 6−12.

[2] YOON Jae-Sik, YANG Jae-Yeol, LEE Ji-Myon, HONG Soon-Jik, HONG Hyun-Seon. A development of the LED TMGa precursor reuse technology [J]. Materials Letters, 2013, 93: 153−156.

[3] MEYER S, WAHL S, MOLCHANOV A, NECKERMANN K, MOLLER C, LAUER K, HAGENDORF C. Influence of the feedstock purity on the solar cell efficiency [J]. Solar Energy Materials and Solar Cells, 2014, 130: 668−672.

[4] LU Fang-hai, XIAO Tang-fu, LIN Jian, NING Zeng-ping, LONG Qiong, XIAO Li-hua, HUANG Fang, WANG Wan-kun, XIAO Qing-xiang, LAN Xiao-long, CHEN Hai-yan. Resources and extraction of gallium: A review [J]. Hydrometallurgy, 2017, 174: 105−115.

[5] KENICHI T, NAGAYASU Y, KISHIO T. Electrolytic refining method for gallium and apparatus for use in the method: United States Patent, US6221232B1 [P]. 2001−04−23.

[6] BOLLONG ALAN B I, BULT ROELOF P, PROUX GARY T. Method for the zone refining of gallium: United States Patent, US23371088A [P]. 1989−12−19.

[7] LEE M S, AHN J G, OH Y J. Production of high-purity indium and gallium metals by vacuum refining [J]. Materials Transactions, 2002, 43: 3195−3198.

[8] PFANN W G. Principles of zone-melting [J]. JOM, 1952, 4: 747−753.

[9] ALEXANDER D V P, ADRIAAN W H. Method for fractional crystallisation of a metal: European Patent, EP20020077683 [P]. 2004−01−13.

[10] VRIES P A D, WOUTERS H A. Method for fractional crystallisation of a molten metal: United States Patent, US7419530B2 [P]. 2008−09−02.

[11] THIEME N, KEIL M, MEIER D, BÖNISCH P, CZARSKE J. Directional solidification of gallium under time-dependent magnetic fields with in situ measurements of the melt flow and the solid-liquid interface [J]. Journal of Crystal Growth, 2019, 522: 221−229.

[12] BELLMANN M P, LINDHOLM D, SORHEIM E A,

MORTENSEN D, MHAMDI M. 3D dynamic simulation of heat transfer and melt flow in an inductively heated crystallization furnace for mc-silicon with PID temperature control [J]. Journal of Crystal Growth, 2013, 383: 119−125.

[13] ZHANG Xiao-xin, FRIEDRICH S, LIU Bin, HUANG Tian-xiang, FRIEDRICH B. Computation-assisted analyzing and forecasting on impurities removal behavior during zone refining of antimony [J]. Journal of Materials Research and Technology, 2020, 9: 1221−1230.

[14] PAN Ke-feng, LI Ying, ZHANG Jia-wei, ZHAO Qing. A facile and low-cost method to produce ultrapure 99.99999% Ga [J]. Materials, 2018, 11: 2308.

[15] DADZIS K, LUKIN G, MEIER D, BONISH P, SYLLA L, PATZOLD O. Directional melting and solidification of gallium in a traveling magnetic field as a model experiment for silicon processes [J]. Journal of Crystal Growth, 2016, 445: 90−100.

[16] PAN K, LI Y, ZHAO Q, ZHANG S. Simulation of solidification process of metallic Ga and its application in preparing 99.99999% pure gallium [J]. JOM, 2019, 71: 737−743.

[17] DANILO C C, SEMIRAMIS F, MICHAEL N, BERND F. Numerical and experimental investigation of germanium refining via fractional crystallization based innovative rotary cooling device [J]. Materials, 2020, 10: 973.

[18] BELLMANN M P, DALAKER H, SYVERTSEN M, GOUTTEBROZE S, MHAMDI M. Optimization of silicon crystallization in a Bridgman growth furnace by numerical modeling [J]. Journal of Crystal Growth, 2013, 362: 38−41.

[19] LU Wen-qiang. Boundary element analysis of the heat transfer in Bridgman growth process of semi-transparent crystals [J]. Materials Science and Engineering A, 2000, 292: 219−223.

[20] NONG X D, JIANG Y L, FANG M, YU L, LIU C Y. Numerical analysis of novel $SiC_{3D}$/Al alloy co-continuous composites ventilated brake disc [J]. International Journal of Heat and Mass Transfer, 2017, 108: 1374−1382.

[21] HOU Jian-feng, PAN Ke-feng, TAN Xi-han. Preparation of 6N, 7N high-purity Ga by crystallization: Process optimization [J]. Materials, 2019, 12: 2549.

[22] KOZLOV S A, POTOLOKOV N A, GUSEV A V, FEDOROV V A. Effect of impurities on crystal growth of Gallium [J]. Inorganic Materials, 2003, 39: 1267−1270.

[23] FARSANI R Y, RAISI A, NADOOSHAN A A, VANAPALLI S. The effect of a magnetic field on the melting of gallium in a rectangular cavity [J]. Heat Transfer Engineering, 2019, 40: 53−65.

[24] KOZLOV S A, POTOLOKOV N A, GUSEV A V, FEDOROV V A. Segregation behavior of impurities in gallium during directional solidification [J]. Inorganic Materials, 2003, 5: 452−454.

[25] BRITIO D, ELBER T D, OLSON P. Experimental crystallization of gallium: Ultrasonic measurements of elastic anisotropy and implications for the inner core [J]. Physics of the Earth and Planetary Interiors, 2002, 129(3): 325−346.

[26] WANG S, FANG H S, WEI G H, ZHOU L, ZHOU N G. Transient analysis of the cooling process and influence of bottom insulation on the stress in the multicrystalline silicon ingot [J]. Crystal Research and Technology, 2013, 48: 454−463.

[27] HOSHIKAWA K, OSADA J, SAITOU Y, OHBA E, MIYAGAWA C, KOBAYASHI T, YANAGISAWA J, SHINOZUKA M, KANNO K. Vertical Bridgman growth of sapphire-seed crystal shapes and seeding characteristics [J]. Journal of Crystal Growth, 2014, 395: 80−89.

[28] KOZLOV S A, POTOLOKOV N A, GUSEV A V, FEDOROV V A. Determination of the effective segregation coefficients of metallic impurities in gallium during directional solidification [J]. Inorganic Materials, 2002, 38(12): 1212−1215.

# 高纯镓轴向结晶提纯过程的数值模拟与实验

丁友东[1,2]，姜 澜[1,2]，李子申[1,2]，付高峰[1,2]，喻 亮[3]

1. 东北大学 多金属共生矿生态化冶金教育部重点实验室，沈阳 110819；
2. 东北大学 冶金学院，沈阳 110819；
3. 桂林理工大学 有色金属及材料加工新技术教育部重点实验室，桂林 541004

**摘 要**：采用瞬态数值模型模拟镓原料在不同冷端温度($T_c$)下的轴向结晶提纯(ADCP)过程，分析熔晶界面形状、温度分布和热应力的变化。结果表明：在 ADCP 过程中，$T_c$ 决定镓材料内部的熔晶界面形状、温度分布和热应力。生长的镓晶体中温度梯度和热应力随着 $T_c$ 的降低而增大。在 $T_c$=15 °C 时，熔晶界面呈现平面或略凸的形状，可为镓材料提供理想的温度梯度、较低热应力、合适的熔晶界面和理想的杂质去除效率。采用 ADCP 工艺在 $T_c$=15 °C 条件下重复 6 次，镓纯度可达到 6N 标准。计算数据与实验数据吻合较好。

**关键词**：高纯镓；轴向结晶提纯；有限元模拟

**(Edited by Bing YANG)**